

Chemical and Dynamical Impacts of Stratospheric Sudden Warmings on Arctic Ozone Variability

S.E. Strahan^{1,2}, A.R. Douglass², and S.D. Steenrod^{1,2}

¹Universities Space Research Association, Columbia, MD

²NASA Goddard Space Flight Center, Atmospheric Chemistry and Dynamics Laboratory, Greenbelt, MD

Main points

Arctic column ozone depletion depends on the number of cold days

Winters with a sudden warming have less than half the depletion of years without one

Dynamics plays a larger role than chemistry in Arctic ozone variability

Abstract. We use the Global Modeling Initiative (GMI) chemistry and transport model with Modern-Era Retrospective Analysis for Research and Applications (MERRA) meteorological fields to quantify heterogeneous chemical ozone loss in Arctic winters 2005-2015. Comparisons to Aura Microwave Limb Sounder N₂O and O₃ observations show the GMI simulation credibly represents the transport processes and net heterogeneous chemical loss necessary to simulate Arctic ozone. We find that the maximum seasonal ozone depletion varies linearly with the number of cold days and with wave driving (eddy heat flux) calculated from MERRA fields. We use this relationship and MERRA temperatures to estimate seasonal ozone loss from 1993-2004 when inorganic chlorine levels were in the same range as during the Aura period. Using these loss estimates and the observed March mean 63-90°N column O₃, we quantify the sensitivity of the ozone dynamical resupply to wave driving, separating it from the sensitivity of ozone depletion to wave driving. The results show that about 2/3 of the deviation of the observed March Arctic O₃ from an assumed climatological mean is due to variations in O₃ resupply and 1/3 is due to depletion. Winters with a stratospheric sudden warming (SSW) before mid-February have about 1/3 the depletion of winters without one and export less depletion to the midlatitudes. However, a larger effect on the spring midlatitude ozone comes from dynamical differences between warm and cold Arctic winters, which can mask or add to the impact of exported depletion.

29 **1. Introduction**

30 The global distribution of stratospheric ozone outside the tropical production region is largely controlled
31 by the circulation. Transport from the tropical middle stratosphere (~5-20 hPa) increases ozone at the
32 poles during winter and spring. In the northern hemisphere, large interannual variability in the strength
33 of planetary waves driving the winter circulation leads to large variability in Arctic spring column ozone
34 [Randel et al., 2002; Weber et al., 2011]. Arctic spring ozone levels began to decline in the 1980s as
35 levels of anthropogenic ozone depleting substances (ODSs) increased, leading to additional Arctic
36 column ozone variability. ODSs are chlorine and bromine-containing compounds with long atmospheric
37 lifetimes that are the sources of most stratospheric reactive halogen species. Ozone depletion each year
38 varies greatly because stratospheric temperature variations affect polar stratospheric cloud (PSC)
39 formation and the subsequent production of reactive halogens. In both hemispheres, winter wave
40 driving controls polar vortex spring temperatures [Newman et al., 2001] and poleward transport of
41 ozone [Randel et al., 2002; Weber et al., 2003]. October (Antarctic) and March (Arctic) mean column O₃
42 (63-90°) determined from satellite observations are often used as indicators of ozone depletion, e.g.,
43 WMO [2014] and prior assessments. Because the Antarctic vortex frequently covers the 63-90°S area
44 and winter ozone resupply is weak and less variable than the Arctic [Weber et al., 2003], the severity of
45 depletion may be qualitatively assessed by the difference between the observed October 63-90°S mean
46 and the estimated pre-1980 climatological value. Determining the degree of anthropogenic ozone
47 depletion based on Arctic March column O₃ variability, however, is problematic because the Arctic
48 vortex is typically smaller than the Antarctic vortex and the 63-90°N area usually includes midlatitude
49 air. In addition, stronger and more variable wave driving in the northern hemisphere leads to large
50 interannual variability in both dynamical resupply and chemical depletion of ozone (e.g., Tegtmeier et
51 al., [2008]).

52 Explaining Arctic spring ozone variability is a prerequisite for detecting changes in polar ozone. ODS
53 levels in the stratosphere have been declining since the late 1990s, but the detection and attribution of
54 an increase in polar ozone due to declining ODSs requires a quantitative separation of chemical
55 depletion from variable seasonal O₃ transport (i.e., dynamical resupply). Some studies have focused on
56 calculating the chemical loss component of spring ozone variability. Ozone losses in the Arctic lower
57 stratosphere have been calculated with sonde data [Rex et al., 2002, and references therein] and with
58 satellite data [Manney et al., 2003; Livesey et al., 2015a] using the 'Match' method that combines
59 observations with reanalysis meteorology in a trajectory model. The trajectory model is used to identify

60 air parcels whose trajectories are inside the vortex. Ozone loss is then calculated as the difference
61 between ozone measurements in the same vortex air parcel on different dates. The accuracy of this
62 method strongly depends on vortex isolation. Rex et al. [2004] calculated vortex-averaged lower
63 stratospheric losses ranging from 20-88 DU from 1992-2002. Livesey et al. [2015a], using Aura MLS O₃
64 data from 2004-2011, calculated losses ranging from 22-116 DU. Other studies have computed lower
65 stratospheric partial column O₃ losses using the tracer-tracer method [Mueller et al., 2001; Tilmes et al.,
66 2003], which assumes a constant relationship inside the vortex between O₃ and a long-lived trace gas,
67 often N₂O, throughout winter. Any mixing across the vortex edge during winter changes the relationship
68 and leads to an underestimate of ozone loss [Mueller et al., 2005], thus this method is best suited for
69 winters with a strongly isolated polar vortex. Livesey et al. [2015a] compared published ozone loss
70 estimates for the winter 2004/5 and noted that the wide range of reported losses indicates the
71 challenge of quantifying ozone depletion in a way that properly accounts for transport processes.

72 Chemistry and transport models (CTMs) integrated with reanalysis meteorology provide an alternative
73 method for assessing ozone depletion by explicitly calculating both the chemical depletion and the
74 transport contributions to Arctic spring ozone. Using CTM simulations of 1991-1998 with and without
75 the effects of chlorine activation on PSCs, Chipperfield and Jones [1999] calculated a 7-yr average
76 column O₃ loss of 38 DU and a mean dynamical resupply of 80 DU. They concluded that the variability of
77 vortex ozone depletion was much smaller than the observed column O₃ variability 63-90°N. However,
78 the results of CTM calculations using reanalyses from more than a decade ago are uncertain because
79 their meteorological fields have excessive mixing and a poor transport circulation due to the assimilation
80 process [Schoeberl et al., 2003; Tan et al., 2004]. Tegtmeier et al. [2008] calculated the contributions of
81 depletion and dynamics to spring column O₃ for 1992-2004 using the Match method for the chemical
82 losses and a reanalysis-derived diabatic descent rate to estimate the dynamical increases in lower
83 stratospheric O₃. They estimated that the O₃ increase due to vortex-averaged diabatic descent varied
84 from 60-140 DU, while chemical depletion varied from 10-100 DU, concluding that the two effects were
85 anti-correlated and contributed equally to Arctic column O₃ variability. Their analysis assumed that the
86 vortex remained isolated through March.

87 It is rare for the Arctic vortex to remain strongly isolated throughout winter. Wave-driven mixing across
88 the vortex edge adds uncertainty to the Match and tracer-tracer methods. Using a 40-yr meteorological
89 reanalysis, Charlton and Polvani [2007] showed that 6 out of 10 winters experienced a major mid-winter
90 stratospheric sudden warming (SSW), defined as a weakening or reversal of the zonal mean zonal wind

91 at 60°N 10 hPa, accompanied by rapid polar warming. SSWs weaken the vortex circulation and allow
92 poleward transport of ozone rich midlatitude air. SSWs also increase temperatures in the lower
93 stratosphere, halting chlorine activation and ozone depletion. The changes in vortex isolation and
94 temperature caused by SSWs clearly affect ozone depletion, but no quantitative relationship has been
95 demonstrated. Manney et al. [2015] report large variability in ozone loss in years with comparable SSWs
96 (2003 and 2010). Kuttipurrath and Nikulin [2012] examined Arctic O₃ depletion from 1994-2010 and
97 concluded that loss was qualitatively proportional to the intensity and timing of SSWs and the volume of
98 polar stratospheric clouds (PSCs), noting that ozone loss in winters with an early season SSW was less
99 than in winters with a late season warming. This suggests a role for SSWs in modulating the impact of
100 polar depletion on midlatitude spring ozone.

101 In this paper, we use the Global Modeling Initiative (GMI) chemistry and transport model with Modern-
102 Era Retrospective Analysis for Research and Applications (MERRA) meteorological fields to quantify the
103 heterogeneous chemical ozone loss in the Arctic for the winters 2005-2015. The methods used here
104 provide a reliable, quantitative approach to separating the chemical and transport contributions to
105 Arctic ozone changes because of the simulation's realistic representation of vortex descent and isolation
106 as well as meridional transport and chemical processes. The methods and model evaluation are
107 described in Section 2 and in the Appendix. In Section 3 we calculate Arctic O₃ depletion for 11 winters
108 and quantify the relationship between depletion, vortex temperature, and eddy heat flux. We show that
109 winters with a SSW have significantly diminished ozone depletion. Section 4 uses the results of Section 3
110 to estimate Arctic spring ozone loss in years 1993-2004, prior to the launch of the Aura satellite (July
111 2004). Using model results and total column O₃ observations, we show distinct relationships between
112 wave driving and ozone depletion, and between wave driving and ozone resupply. Section 5 shows how
113 depletion and O₃ transport have different spatial impacts on midlatitude ozone and surface UV in spring,
114 depending on the occurrence of a midwinter stratospheric sudden warming. The results of this study are
115 summarized in Section 6.

116 **2. Observations, the GMI Model, and Methods**

117 This study uses Aura Microwave Limb Sounder (MLS) v4.2 Level 2 profile measurements of O₃ between
118 October 2004 and May 2015 (Livesey et al., 2015b); they are reported on a vertical resolution grid with
119 12 pressures per decade. We calculate MLS ozone columns using levels 268-0.46 hPa and refer to them
120 as the stratospheric column; the reported 2 σ column accuracy is 4%. The 268 hPa level is generally near
121 the tropopause inside the vortex. MLS v3.3 N₂O and temperature data from October 2004 to May 2013

122 are used for CTM transport evaluation in the lower stratosphere (46-100 hPa), where the N₂O 2σ
123 accuracy is 14% (Livesey et al., 2011). The primary MLS band used to retrieve N₂O failed in June 2013.
124 Ongoing retrievals using Band 3 (190 GHz) are scientifically useful from 68-0.46 hPa but are high biased
125 and noisy at 68 hPa. The transport evaluation is therefore restricted to dates before the primary band
126 failure. We also use satellite observations of March total column O₃ from the NASA GSFC Ozone and Air
127 Quality website (<http://ozoneaq.gsfc.nasa.gov/>). The column O₃ data sets we use cover the period 1979
128 to the present nearly continuously and consist of measurements from several different instruments,
129 from the Total Ozone Mapping Spectrometer (TOMS) on Nimbus-7 to the Ozone Measuring Instrument
130 (OMI) on the NASA Aura satellite.

131 The GMI CTM was integrated from January 1, 2004-May 31, 2015 using MERRA reanalysis
132 meteorological fields (Rienecker et al., 2011) with 1°x1.25° horizontal resolution and 72 vertical levels
133 having ~1 km resolution between 300-10 hPa. Details of the GMI CTM and this simulation are found in
134 Strahan et al. [2013] and references therein. For the period of the simulation, all organic halogen
135 species and other long-lived species are forced by appropriately changing mixing ratios at the surface. In
136 addition, a second GMI simulation ('No Het') was integrated with the rates for heterogeneous reactions
137 involving chlorine and bromine set to zero for the months October to May. This eliminates halogen
138 activation by all PSC particle types. Both simulations have the same transport because they are
139 integrated with the same MERRA meteorology and there is no feedback between simulated O₃ and
140 dynamics. The 'No Het' simulation is initialized on October 1 each year with conditions from the full
141 chemistry simulation. The difference in O₃ fields between the 'No Het' and the full chemistry simulation
142 measures the heterogeneous chemical loss independent of dynamical changes in O₃.

143 A CTM experiment requires the realistic representation of ozone loss processes and transport over the
144 course of winter to accurately calculate polar O₃ change. A simulation must, for example, closely
145 reproduce long-lived tracer observations inside the vortex to demonstrate that isolation and descent are
146 well-represented. This is critical for simulating the dynamical supply of ozone. Strahan et al. [2013]
147 demonstrated the transport and chemistry credibility of this GMI simulation by showing close
148 agreement between this simulation and MLS N₂O, O₃, and ClO profiles inside the Arctic vortex during the
149 winter of 2011. In the Appendix we demonstrate the fidelity of this simulation throughout the Aura
150 period using comparisons with observations in 4 winters with widely varying Arctic vortex strength. The
151 comparisons to MLS N₂O in Figure A1 verify that before the final warming, the simulation produces
152 realistic transport in the Arctic lower stratosphere whether the vortex is strong or weak. The lower

153 panels of Fig. A1 show that the simulated column O_3 changes closely track the MLS O_3 changes.
154 Together, the N_2O and O_3 comparisons demonstrate the credibility of this simulation's net
155 heterogeneous chemical loss and its high latitude circulation and mixing.

156 The simulation is limited to the period of the Aura satellite, 2004–2015, for reasons related to MERRA
157 transport fidelity prior to Aura. Aura MLS observations provide the first global daily profile datasets of
158 ozone and a long-lived source gas (N_2O). Abalos et al. [2015] compared the Brewer Dobson Circulation
159 (BDC) obtained from three modern reanalyses including MERRA, and showed substantial differences in
160 the tropical upwelling (up to 40%). Although they do not evaluate the BDC in polar regions or the
161 representation of the polar vortex and its isolation, such a large level of uncertainty in the BDC indicates
162 the necessity of a dataset like MLS for evaluation. Comparisons of MERRA-driven simulations in the
163 1990s with datasets from the Upper Atmosphere Research Satellite (UARS) instruments such as the
164 Cryogenic Limb Array Etalon Spectrometer (CLAES) and the HALogen Occultation Experiment (HALOE)
165 reveal issues with the subtropical gradients in long-lived tracers and a poor representation of the effects
166 of the quasi-biennial oscillation. Our evaluation of MERRA's circulation prior to Aura suggests caution
167 and comprehensive evaluation is not possible. Note that we use $v'T'$ computed from MERRA for 1993–
168 2004; this product of deviation from the mean is much more certain than the residual circulation fields,
169 v^* and w^* .

170 The constituent analyses use the equivalent latitude/potential temperature coordinate system
171 calculated from daily MERRA potential vorticity (PV) and temperature fields. Potential vorticity is a good
172 tracer of atmospheric motions because it is conserved on a timescale of weeks in the lower
173 stratosphere. Equivalent latitude is calculated by mapping daily PV fields (on potential temperature
174 surfaces) onto equal areas centered on the pole; the same mapping is then applied to a trace gas field,
175 creating a vortex-centered coordinate [Nash et al., 1996]. This mapping allows the definition of a
176 dynamical boundary between the polar vortex and midlatitude air masses, advantageous for studies of
177 polar processes such as ozone depletion [Manney et al., 2003, Mueller et al., 2008]. We use an Arctic
178 cap average, defined as the area-weighted mean over 63-90°N equivalent latitude (EqL), to analyze polar
179 processes. MLS and GMI stratospheric ozone columns are calculated using the same pressure range,
180 268-0.46 hPa. MERRA zonal wind and temperature are also used to identify minor and major SSWs.
181 MERRA minimum temperatures in the Arctic winter lower stratosphere have been shown to agree
182 within 1 K with ERA-Interim temperatures after 1997 and to within 1.4 K before that [Lawrence et al.,
183 2015]. The dynamical analyses use the daily 100 hPa zonal mean eddy heat flux, $v'T'$, averaged from 45-

184 75°N over the preceding 45 days; it is available from the NASA Goddard data services website
185 (http://acdb-ext.gsfc.nasa.gov/Data_services/met/ann_data.html). The 45-day averaging comes from
186 the radiative damping timescale in the lower stratosphere, as used in Newman et al. [2001].

187 **3. Dynamical Control of Ozone Depletion, 2005-2015**

188 Temperature and ODS levels are the primary factors controlling polar ozone depletion [Newman et al.,
189 2004]. Levels of stratospheric inorganic chlorine (Cl_y) have declined roughly 8% between 2005 and 2015
190 due to declining ODS levels, but Cl_y in the winter polar lower stratosphere remains above 2.5 ppb, a level
191 50% greater than 1980 values [Strahan et al., 2014]. Because year-to-year variations in Cl_y levels are
192 small, temperature variations exert primary control over interannual variations in polar ozone depletion
193 [Newman et al., 2006]. This analysis investigates the influence of dynamics on ozone depletion through
194 vortex stability and temperature.

195 **3.1 Quantifying Arctic Ozone Loss**

196 In this section we calculate the column O_3 change due to heterogeneous chemical loss in all Arctic
197 winters 2005-2015 using the difference between the GMI full chemistry and ‘No Het’ simulations. The
198 column O_3 differences between these simulations provide a daily look at ozone depletion throughout
199 the Arctic that cannot be obtained by observations alone. Figure 1 shows the maximum seasonal
200 depletion in 4 years with widely varying dynamical conditions. The top panels show years where a SSW
201 caused a split (2013) or displaced (2010) vortex, leading to high temperatures that ended ozone
202 depletion by midwinter. The lower panels show two cold, weakly disturbed years with a mid-March
203 (2005) and a mid-April (2008) final warming. Maximum local losses in these two years without a SSW
204 were greater than 60 DU while the disturbed winters had a maximum loss near 30 DU. The greatest
205 losses of this decade were shown in Strahan et al. [2013], when local losses exceeded 100 DU in late
206 March 2011.

207 The equivalent latitude coordinate (EQL) accounts for variations in vortex size and shape, allowing the
208 magnitude of depletion to be easily compared each year. Figure 2 shows 11 years of daily ozone
209 depletion mapped onto equivalent latitude using MERRA potential vorticity on the 450 K isentropic
210 surface. The 450 K surface is near the midpoint of the altitude range of ozone depletion (~350-540 K, or
211 150-30 hPa). Figure 2 shows that O_3 depletion varies greatly over the 11 years, with maximum losses
212 each year ranging from 21 to 93 DU. The region of steep O_3 loss gradients is generally co-located with
213 the vortex edge. These gradients are found at the lowest latitudes in 2005 and 2014, indicating a very
214 large vortex.

215 The patterns in Figure 2 fall into two groups based on the timing and magnitude of the loss. Five years
216 (2005, 2007, 2008, 2011, and 2014) maintain losses of more than 40 DU for at least 6 weeks, with a
217 maximum loss of >50 DU occurring in March. The other 6 years have a maximum loss less than 40 DU,
218 and except for 2015, the maximum occurs in January or February. In all years the maximum loss occurs
219 north of 80° EqL. The years with high losses also have higher losses at lower latitudes. The high loss
220 group has losses of 25-50 DU at 70° EqL, while the losses there never exceed 25 DU in the low loss
221 group. The high loss group also stands out in April because losses >5 DU appear south of 50° EqL.

222 Figure 3 shows the daily Arctic cap mean, defined as the area-weighted mean depletion between 63-90°
223 equivalent latitude, to summarize the year-to-year depletion variations shown in Figure 2. This quantity,
224 used in previous studies (e.g., Mueller et al, [2008]; WMO [2014]), captures essentially all of the ozone
225 loss that occurred inside the vortex shown in Fig. 2. There are many similarities each year in the
226 evolution of Arctic cap loss. Depletion in December is small: ≤1 DU before the 10th and still less than 4
227 DU in most years by the end of the month. Very low temperatures that persisted throughout a deep
228 layer of the lower stratosphere in December 2012 led to a higher early season loss rate in 2013 than
229 other years [Manney et al. 2015]. By the end of January, all years have 11-18 DU loss, except 2015,
230 which had warm early winter temperatures that delayed the onset of depletion. But in February there
231 are large year-to-year variations in losses and by March 1, the losses have separated into two groups: 6
232 years with maximum losses from 12-22 DU (dashed lines), and 5 years with losses from 30-52 DU (solid).
233 The mean loss in the high loss group (41 DU) is nearly three times greater than the mean of the low loss
234 group (16 DU).

235 **3.2 Ozone loss and Heat Flux**

236 It is well-known that polar ozone depletion is controlled through the temperature-dependence of PSC
237 particle formation and the subsequent production of active forms of chlorine and bromine [Kawa et al.,
238 1997]. Wohltmann et al. [2013] showed there is a strong linear relationship between chlorine activation
239 and column O₃ loss, and that modelled loss was insensitive to the details of the chlorine activation (i.e.,
240 particle type). We look for a relationship between the maximum Arctic cap ozone loss shown in Figure 3
241 and the number days with lower stratospheric vortex temperatures below the threshold for particle
242 formation. We use MERRA temperatures and the Hanson and Mauersberger [1988] kinetics constants to
243 calculate the temperature thresholds for particle formation on 5 MERRA pressure levels from 150-30
244 hPa. We count the number of days each season with below-threshold temperature anywhere inside the
245 vortex on at least 2 pressure levels. The area of below-threshold temperatures is not considered, and

246 only days after December 15th are counted because there is negligible loss before. Figure 4a shows a
247 highly correlated (0.97) approximately linear relationship between the maximum seasonal Arctic cap
248 column O₃ depletion and the number of days when vortex temperatures were at or below particle
249 formation temperatures on at least 2 pressure levels. A similar relationship, but with greater scatter, is
250 found when we require below-threshold temperatures on only 1 level. Similar results would likely be
251 obtained using the ERA-Interim reanalysis. Lawrence et al. [2015] showed that the number of days each
252 Arctic winter with temperatures below the PSC activation threshold in MERRA agreed to within a few
253 days to the number found in ERA-Interim from the 1980s to the present.

254 Figure 4a shows that the severity of seasonal Arctic ozone loss can be estimated to within ± 6 DU based
255 on the number of cold days inside the vortex. The loss rate is ~ 0.5 DU loss/cold day over a range of 12-
256 52 DU loss for 2005-2015, for current high Cl_y conditions in the polar lower stratosphere (mean age ~ 5
257 yrs). Over the past decade Antarctic Cl_y has been estimated to vary between 2.55-2.95 ppb [Strahan et
258 al., 2014]. We expect Arctic Cl_y values to be similar because the mean age and the age spectrum of the
259 Arctic lower stratosphere are similar to the Antarctic [Li et al., 2012]. As ODS levels slowly decline, the
260 slope of this line will flatten [Weber et al. 2011]. The Cl_y decline rate of less than 1%/yr is too slow to
261 have a discernable effect on the fitted slope, which has 1σ uncertainty of 10%.

262 This result is similar to the relationship found by Rex et al. [2004] between the Arctic column ozone
263 depletion and the volume of air with seasonally-averaged (December-March) temperatures below PSC
264 thresholds (V_{psc}). Our result suggests that the key factor to loss is the *duration* of low temperatures
265 rather than their *volume*. Duration is implicitly a factor in their result because they used a seasonal
266 average of vortex temperatures, however, because V_{psc} depends on the area of low temperatures while
267 our metric does not, a given V_{psc} does not uniquely correspond to the number of cold days; the
268 correlation of V_{psc} and cold days during the Aura period is 0.74. We find a correlation of 0.97 between O₃
269 loss and the number of cold days (Fig. 4a), and a significant but lower correlation between O₃ loss and
270 V_{psc} , 0.85. Our results for the seasonal maximum loss averaged over 63-90°N EqL are roughly half the
271 loss estimates reported for 2005-2011 by Livesey et al. [2015a] using MLS O₃ measurements and the
272 Match method. They report that ozone loss estimates are sensitive to the value of potential vorticity
273 chosen to define the vortex edge by affecting the area over which losses are averaged. For this reason,
274 the conservative potential vorticity criteria they apply to their matches are likely to result in larger loss
275 estimates than ours because they average over higher equivalent latitudes where losses are greater.
276 They note that when the vortex is disturbed, meridional transport and mixing will lead greater error in

277 their estimates. Our method properly accounts for those contributions to Arctic O₃ regardless of the
278 degree of disturbance.

279 Newman et al. [2001] demonstrated that the strength and temperature of the polar lower stratospheric
280 vortex are controlled by planetary wave driving, finding a relationship between the mean midwinter 100
281 hPa eddy heat flux from 45-75°N ($v'T'$) and the March 50 hPa temperature 60-90°N. The eddy heat flux is
282 proportional to the vertical component of the Eliassen-Palm flux, which we use here as a measure of
283 planetary wave driving. Figures 4b and 4c show that the number of cold days and the maximum
284 seasonal heterogeneous chemical loss, both driven by temperature, are strongly correlated with the 100
285 hPa heat flux averaged over the period where most depletion occurs (mid-December through February).
286 Figure 4b shows that years with a larger numbers of cold days are associated with lower heat fluxes,
287 consistent with the results of Newman et al. [2001] that showed weak wave driving leads to a stable,
288 long-lived vortex. 2011 had the greatest number of days with temperatures below PSC thresholds and is
289 tied with 2005 for the weakest wave driving (Dec 15-Feb 28 average) of the Aura period.

290 **3.3 The Impact of Stratospheric Sudden Warmings on O₃ Depletion**

291 Six of 11 recent winters had much less seasonal loss, fewer cold days, and stronger wave driving than
292 the other years. Strong wave driving can lead to a stratospheric sudden warming, defined as the reversal
293 of the zonal mean zonal wind at 10 hPa and 60°N, accompanied by a rapid reversal of the poleward
294 zonal mean temperature gradient [Andrews et al., 1987]. The warming is minor when the temperature
295 gradient reverses but the zonal wind does not. The warming is final if the return to westerly zonal winds
296 lasts fewer than 10 consecutive days [Charlton and Polvani, [2007]. We use these criteria and MERRA
297 wind fields to assess Arctic winters 2005-2015. The years 2006, 2009, and 2013 are at the low loss end of
298 Figure 4a (<15 DU) and all experienced a January major SSW with a wind reversal persisting at least 3
299 weeks. The years 2010 and 2012 had minor warmings that did not quite attain the major SSW definition,
300 but had westerlies that dropped from ~40 m/s to 10 m/s or less for a month or more. The minor
301 warming in early January 2015 had 10 hPa 60°N winds that dropped from 40 to ~20 m/s for more than a
302 month. These six years with SSWs averaged 37 days sufficiently cold for Cl activation and had seasonal
303 Arctic cap losses of 12-22 DU.

304 None of the 5 high loss years (2005, 2007, 2008, 2011, and 2014) had a major or minor warming before
305 mid-February. The 60°N 10 hPa winds in these 5 years remained high (>20 m/s) from December through
306 mid-February or later and had temperatures that were usually near or below average. These conditions
307 led to a vortex that was relatively undisturbed until late winter, allowing Cl activation to persist roughly

308 6 weeks longer than the disturbed winters. These years experienced Arctic cap maximum losses of 30-52
309 DU.

310 We use the occurrence of a stratospheric sudden warming, major or minor, before late winter to divide
311 the years 2005-2015 into two groups. Figure 5 shows the mean differences in the magnitude, timing,
312 and midlatitude impact of Arctic ozone depletion in winters with a SSW (referred to as warm or
313 disturbed) and those with a more stable vortex (referred to as cold or stable). The means are calculated
314 from the results in Figure 2. In disturbed years, a mean maximum loss of 22 DU occurs north of 84°
315 equivalent latitude in mid-February. The impact on the midlatitudes in spring is small, on average less
316 than 5 DU south of 50°. By early May there are no losses greater than 10 DU at any latitude. In contrast,
317 years with a stable vortex have an average maximum loss nearly 3 times greater, 62 DU, that occurs
318 about a month later than the disturbed years. The larger magnitude, larger areal extent, and late March
319 timing of the maximum loss can result in a larger impact on lower latitudes in spring when surface UV
320 levels are rapidly increasing. Ozone depletion at polar latitudes in April is also substantially greater in
321 cold years (~15-57 DU) compared to disturbed years (10-18 DU). By May all losses have diminished but
322 cold year losses remain about twice the size of disturbed year losses.

323 **4. March Arctic Ozone Variability, 1993-2015**

324 Figure 3.4 in Chapter 3 of the WMO Ozone Assessment [, 2014] shows large year-to-year variability in
325 Arctic March mean total column O₃ in the past 30 years, with some values more than 100 DU below the
326 figure's implied climatological mean value of 455 DU. We calculate the March average loss over the
327 geographic (*i.e.*, not equivalent latitude) Arctic cap for 2005-2015; this is the same space and time
328 averaging used in the WMO Assessment. This area-averaged loss also has a linear relationship with the
329 number of cold days, and we use this relationship and meteorological data to estimate losses for 1993-
330 2004. By adding the estimated loss to observed March O₃ from 1993-2015, we determine a relationship
331 between wave driving and March O₃ in the absence of halogen catalyzed ozone loss. The results
332 presented here quantitatively explain the sources of observed Arctic March O₃ variability. GMI-MERRA
333 simulations cannot be used to quantify ozone depletion during the 1990s because of known
334 uncertainties in the MERRA transport circulation described in Section 2 and the lack of satellite
335 measurements needed for a comprehensive evaluation of polar ozone transport.

336 **4.1 Estimation of March Arctic Ozone Depletion before Aura**

337 To understand the variability caused by depletion in the multi-decadal March Arctic O₃ record, we
338 calculate the March monthly mean column O₃ depletion from the GMI simulations, 2005-2015, averaged

339 over 63-90°N geographic latitude as in WMO [Dameris and Godin-Beekmann, 2014]. Figure 6a shows a
340 highly correlated relationship, similar to Fig. 4a, between the mean March 63-90°N depletion and
341 number of cold days. We use the slope of the line in Fig. 6a to estimate the March depletion in the years
342 prior to Aura. The number of cold days inside the vortex each year from 1993-2004 was determined
343 from MERRA temperatures and potential vorticity (to identify the vortex), using the same criteria
344 described in Section 3. Using the slope in Fig. 6a and the number of cold days each year, we estimate the
345 March average 63-90°N ozone depletion for years 1993-2004. This is shown in Figure 6b along with the
346 loss values for 2005-2015 (from Fig. 6a). We exclude years prior to 1993 from this analysis because polar
347 lower stratospheric Cl_y is estimated to be lower than 2004-2015 levels [Newman et al., 2007] and the
348 relationship between depletion and cold days (Fig. 6a) would have a different slope. None of the years
349 1993-2004 had more cold days than the coldest Aura year (2011) and 3 had fewer cold days than the
350 warmest Aura year (2013). The estimated losses from 1993-2015 range from 1-39 DU, with an average
351 of 18 DU. Based on the deviations from the linear fit shown in Fig. 6a, the 2σ uncertainty of the loss
352 estimates is 5.5 DU.

353 Figure 7 shows the time series of observed Arctic March O_3 from TOMS and OMI instruments from 1979-
354 2015. The red dashed line is the March mean heterogeneous loss (from Fig. 6b) added to the observed
355 March column O_3 ; it is referred to as 'No Het Loss' O_3 . The losses are shaded in blue. The yellow shading
356 represents the difference between the estimated March 'No Het Loss' O_3 and the 455 DU 'climatological
357 mean' value implied by WMO Figure 3.4. This figure reveals that depletion usually accounts for less than
358 half the difference between 455 DU and the observations. The average 'No Het Loss' March O_3 ranges
359 from 375 to 464 DU, averaging more than 30 DU below the implied climatological mean. As a result, the
360 observed March O_3 in the WMO figure gives the impression of much greater depletion than actually
361 occurs. By calculating the percentage of March ozone loss with respect to the 'No Het Loss' O_3 values
362 determined here (rather than 455 DU), we find the largest depletion of the 1993-2015 period is 10% in
363 2011; the average is 4.4%. Even with a 5.5 DU 2σ loss uncertainty, depletion (blue shading) usually
364 accounts for less than half of the observed difference from 455 DU (blue and yellow together). This is
365 shown as the depletion fraction at the bottom of the figure.

366 **4.2 Sensitivities of O_3 Resupply and O_3 Depletion to Wave Driving**

367 Quantitatively separating wave driving's effect on ozone resupply from its effect on ozone depletion is
368 challenging because polar ozone is affected by each process in the same sense: stronger wave driving is
369 associated with increased ozone (increased resupply and reduced loss) whereas weaker wave driving is

370 associated with decreased ozone (reduced resupply and increased loss). Total column O₃ observations
371 from 1993-2015 and the 'No Het Loss' O₃ time series provide a way to separate polar ozone sensitivities.
372 We use the 45-75°N mean 100 hPa heat flux averaged from December through March as a measure of
373 the strength of the wave driving that affects March ozone. Figure 8a shows the relationship between
374 wave driving and March 'No Het Loss' O₃, which reflects the sensitivity of resupply to dynamics in the
375 absence of depletion. The relationship is highly correlated (0.73) and the slope of the best fit line is 11.7
376 ± 2.0 DU/Kms⁻¹. Figure 8b shows the relationship of wave driving and the March O₃ observations, which
377 indicates the combined sensitivity of resupply and depletion to dynamics. The correlation of these
378 points is 0.79 and the slope is 16.4 ± 2.2 DU/Kms⁻¹. Fall wave driving is small compared to winter and its
379 inclusion in the analysis period does not increase the correlation. The range and mean of the heat fluxes
380 from 1993-2004 (open symbols) are approximately the same as the range and mean of the Aura period
381 (solid symbols), indicating no trend in wave driving during this 23 year period that might affect observed
382 Arctic O₃ variability.

383 The difference of the slopes in Fig. 8b, 4.7 ± 3.0 DU/Kms⁻¹, represents the sensitivity of O₃ depletion to
384 variations in the heat flux during the past two decades while Cl_y has been high relative to 1980 levels.
385 The ozone value where the two lines intersect, 460 DU, represents the point where wave driving is
386 sufficient to inhibit heterogeneous loss, and is very close to the implied climatological mean value used
387 in WMO Figure 3.4. This analysis shows that O₃ resupply is roughly twice as sensitive to wave driving as
388 depletion is (11.7 compared to 4.7 DU/Kms⁻¹). The attribution of an Arctic ozone increase to declining
389 halogens will be very difficult because of the relative size of these sensitivities. Most of the difference
390 between the observed O₃ record and 455 DU is due to the variability of resupply, not depletion. Given
391 the slope uncertainties, depletion therefore explains about 30 (±20)% of the observed difference from
392 455 DU. In other words, depletion accounts for at most half, but more likely less than half of the
393 difference from 455 DU, with the remainder of difference coming from variability in the wave-driven
394 supply of O₃. Bednarz et al. [2016] found that ozone depletion contributed ~30% to March Arctic ozone
395 variability in a 100-yr simulation with the UM-UKCA chemistry climate model, concluding as we do that
396 dynamical variability is the primary contributor to interannual variations in Arctic spring column O₃.

397 Tegtmeier et al. [2008] performed a similar analysis to determine dynamical supply and depletion
398 sensitivities to wave driving from December to mid-March, 1992-2004. They concluded that inside the
399 vortex those sensitivities were the same. Their method to estimate the dynamical contribution to polar
400 O₃ explicitly neglected meridional mixing into the vortex as well as column O₃ changes above 550 K (30

401 hPa). Their depletion was calculated with the Match method using O₃ sondes and a trajectory model
402 [Rex et al., 2006]. As discussed in Livesey et al. [2015a], meridional transport and mixing add uncertainty
403 to the Match calculation of vortex-averaged chemical loss. Although we find similar year-to-year loss
404 variability, our results differ from Tegtmeier et al. [2008] in part because we are calculating the March
405 mean total column O₃ 63-90°N, which includes some non-vortex air, rather than a vortex-averaged
406 quantity. But differences are also likely because our method accounts for rather than neglects O₃
407 changes due to transport and mixing.

408 **5. The Net Effect of Dynamics and Depletion on April O₃**

409 This study has two key findings that are relevant to understanding midlatitude spring O₃ variability. First,
410 most of the interannual variability in the Arctic March mean O₃ comes from resupply variability rather
411 than depletion. And second, the seasonal ozone depletion in years with a cold, stable vortex is on
412 average 3 times greater and occurs one month later (March) than disturbed years. In this section we
413 examine the effects of these findings in April and consider the spatial variations of their effects on
414 midlatitude O₃ and surface UV index (UVI) variability. We calculate the MLS total column O₃ by
415 combining MLS stratospheric column O₃ with the GMI tropospheric O₃ column. We also calculate a 'No
416 Het Loss' MLS O₃ column by adding GMI-calculated depletion to the MLS total column.

417 Figure 9 looks at differences in the effects of depletion (top row) and resupply (bottom row) to the April
418 mean total column O₃ north of 20°N after cold and warm winters. Figures 9a and 9b show the net
419 change due only to depletion in cold and warm years, and Fig. 9c shows the difference between them.
420 The Aprils that follow a cold winter have 10-20 DU greater depletion over northern Europe and Asia (0-
421 130°E) and up to ~5 DU greater depletion over North America (near 250°E) than those following warm
422 winters; the white boxes on panels c and g indicate the European and North American regions. Panels in
423 the bottom row, Figs. 9e-h, are calculated with the MLS 'No Het Loss' column O₃. Figs. 9e and 9f show
424 the April total column O₃ distributions after warm and cold winters; Fig. 9g shows the mean differences
425 between them, due only to dynamics. There is large longitudinal variability. Dynamics contributes up to
426 18 DU more and up to 30 DU less O₃ at certain longitudes between 50-70°N after cold winters. This is
427 often larger than the depletion differences in Fig. 9c (directly above Fig. 9g).

428 Figures 9c (depletion) and 9g (dynamics) show the different causes of column O₃ variability after cold
429 and warm winters. Their net effect varies strongly with region. Consider the boxes drawn on these
430 panels, representing the locations of many ground-based measurements stations in Europe (longitudes
431 0-30°E) and North America (longitudes 235-290°E). Over Europe the net effect in April after cold years is

432 8-18 DU lower O₃ than in warm years, with similar contributions from depletion and dynamics. But over
433 North America, while there is some O₃ depletion (Fig. 9c) there is a greater increase in O₃ supply (Fig.
434 9g), with the net effect that O₃ is up to 10 DU higher after cold years. Ground-based column O₃
435 measurements from Europe and North America will show different April variability due to longitudinal
436 variations in O₃ transport and the export of polar O₃ depletion.

437 To assess the significance of Arctic ozone loss on surface UV, we calculate the clear sky impact on the
438 surface UV index from the O₃ changes shown in Fig. 9c and 9g using a lookup table of UVI as a function
439 of overhead ozone and solar zenith angle [Newman and McKenzie, 2011]. The right-hand side panels
440 (Figs. 9d and 9h) show how depletion and dynamics affect the April UVI differently after cold and warm
441 winters. Typical April mean clear sky UV indices range from 10 at 30°N to 3 at 60°N (not shown).
442 Depletion has small impacts on UVI in April, 0.1-0.2 after cold winters and 0-0.1 after warm winters; the
443 difference in their impact is 0-0.1 (Fig. 9d). Although there are large differences in depletion after warm
444 and cold winters (Figs. 9a and 9b), the impact on UVI at polar latitudes is negligible due to low solar
445 zenith angles in early spring. In the midlatitudes, sun angles are higher but the depletions are <10 DU in
446 both cold and warm winters, thus the impact of depletion on UVI is small here too, <0.2. However, the
447 cold-warm dynamical differences in the midlatitudes are much larger than depletion differences (Fig.
448 9h). They show a larger increase in surface UVI, up to 0.3 over Asia (70-130°E), but a lower UVI over
449 North American longitudes after cold Arctic winters. Overall the effects of Arctic ozone depletion on
450 April surface UVI are small. The primary source of clear sky April UVI variability in the mid and high
451 latitudes is column O₃ dynamical variability.

452 **6. Summary and Conclusions**

453 We used realistic simulations from the GMI CTM with and without heterogeneous halogen chemistry to
454 quantify the heterogeneous chemical loss and the dynamical contributions to March Arctic ozone for the
455 winters 2005-2015. We found that the maximum Arctic O₃ loss each season, averaged over 63-90°
456 equivalent latitude, depends linearly on the number of days that lower stratospheric vortex
457 temperatures were below the threshold for halogen activation on PSC particles. The occurrence of a
458 stratospheric sudden warming strongly influences the number of cold days in the vortex. Winters with a
459 major SSW had the fewest cold days and the least O₃ loss, while years with no major or minor warming
460 before mid-February had the most cold days and the greatest O₃ loss. From 2005-2015, 5 years had
461 weak wave activity and a persistently cold vortex. The average O₃ loss in those years was nearly 3 times
462 greater than years with a minor or major SSW, and the areal extent of the loss was also greater. The

463 maximum O₃ loss in cold years occurred in mid-March, approximately 1 month later than the warmer
464 years. All of these factors led to greater export of ozone depleted air to the midlatitudes in years with a
465 cold and weakly disturbed polar vortex. Aprils following a disturbed winter vortex have 2-8 DU
466 depletions between 30°-60°N while Aprils following a cold vortex have an average depletion of 5-15 DU.
467 Even after cold winters, depletion has a very small impact on surface UVI in April, causing on average
468 less than a 0.2 increase in surface UV index at any latitude, and generally less than 0.1.

469 Dynamically-driven (i.e., transport) differences in the O₃ distribution between warm and cold Arctic
470 winters have a much larger effect on mid and high latitude spring O₃ than does the export of polar
471 depletion. Some longitudes will have lower O₃ after cold winters due to a combination of depletion and
472 dynamics, while other longitudes will have higher O₃ because a positive dynamical contribution
473 dominates a small depletion. Trends calculated from ground-based column O₃ measurements in the
474 northern mid and high latitudes may be affected by the large longitudinal variations in the sources of O₃
475 variability. Observed variability at European and North American sites will reflect different contributions
476 from ozone-depleted air and from transport, with neither location representative of the zonal mean.

477 The quantitative relationship identified between cold days and ozone depletion during the Aura period
478 made it possible to estimate Arctic spring ozone loss from 1993-2004 using MERRA temperatures. With
479 these estimated O₃ depletions, we produced a record of Arctic March 'No Het Loss' total column O₃ for
480 1993-2015 averaged over 63-90°N geographic latitude, the same averaging used in the WMO
481 Assessment. Each year the March observed O₃ and 'No Het Loss' O₃ vary, but the difference in their
482 sensitivities to wave driving revealed the sensitivity of depletion, independent of resupply. For every 2
483 DU that wave driving increases resupply there is about a 1 DU decrease in depletion. From 1993-2015,
484 dynamical contributions to March ozone varied by 80 DU while chemical depletion reduced O₃ between
485 1 and 39 DU. The largest depletion of this period, 10%, occurred in 2011 when the March mean loss was
486 39 DU while weak resupply reduced the 'No Het Loss' O₃ to 379 DU. Although our results are consistent
487 with previous estimates of the contributions of depletion and resupply to Arctic O₃ (Tegtmeier et al.,
488 [2008]; Chipperfield and Pyle [1999]), they represent an improvement because our methods better
489 account for vortex O₃ changes due to transport.

490 Our results explain the variability in the WMO Arctic O₃ record. Because wave driving controls both the
491 O₃ resupply (via transport) and O₃ depletion (via temperature), winters with weak wave driving (smaller
492 resupply) will have a colder, more stable vortex with greater heterogeneous ozone depletion compared
493 to winters with stronger wave activity. The 455 DU climatological March mean suggested by Figure 3.4

494 of WMO [Dameris and Godin-Beekmann, 2014] masks the importance of dynamical variability in
495 determining Arctic spring O₃ each year; it is at the high end of the 375-464 DU range we find for 1993-
496 2015 ('No Het Loss' O₃). In the future when anthropogenic ODSs are significantly lower than today,
497 interannual variability in wave driving will continue to produce large variability in Arctic March O₃.
498 Using the relationship found in this study between cold days and ozone depletion, we estimate that the
499 Arctic winter of 2016 had a 63-90°N EqL seasonal maximum O₃ depletion of about 40 DU. MERRA shows
500 that the low temperatures required for depletion persisted in the 2015/2016 Arctic vortex for 84 days,
501 about the same as 2005 and 2014. The winter of 2011 had 105 days (3.5 months) with temperatures low
502 enough for chlorine activation, the most in the 1993-2015 record examined here.

503 With inorganic chlorine levels declining, it is unlikely that future Arctic winters will exceed the 2011
504 ozone loss, however, the decadal scale impact of depletion could increase. From 2005-2015, the mean
505 maximum Arctic cap ozone depletion for equivalent latitudes 63-90°N was 28 DU and it was modulated
506 by the frequency of SSWs: 6 of 11 recent winters had a major or minor warming before mid-February
507 that kept depletion below 22 DU. This frequency is similar to that reported by Charlton and Polvani
508 [2007] based on 40 years of reanalyses. Within that 40-year period they found large decadal scale
509 variability in SSW frequency, with an SSW in every year of the 1980s but only 2 in the 1990s. In spite of
510 the projected decline in polar stratospheric Cl_y levels of ~22 ppt/yr [Strahan et al., 2014], Cl_y levels
511 during the next two decades will remain above 2 ppb, enough to cause significant ozone depletion. If
512 the coming decades experience a reduced frequency of SSWs similar to the 1990s, Arctic ozone
513 depletion may appear to become a more serious problem in spite of declining chlorine levels. The
514 improved understanding of the role of dynamics in winter and spring O₃ distributions gained in this
515 study will allow a more accurate attribution of sources of O₃ variability in future observations.

516

517 **Acknowledgments.** This work was supported by the NASA Modeling, Analysis, and Prediction Program
518 and the NASA Atmospheric Composition Modeling and Analysis Program. MLS data are available at
519 <http://mls.jpl.nasa.gov>. The MERRA reanalysis can be obtained from the Goddard Earth Science Data
520 and Information Services Center, <http://disc.sci.gsfc.nasa.gov/daac-bin/DataHoldings.pl>. Derived
521 meteorological quantities such as heat fluxes can be obtained through this NASA data services website
522 (http://acdb-ext.gsfc.nasa.gov/Data_services/met/ann_data.html). GMI simulation output is available
523 by request to susan.e.strahan@nasa.gov. We thank the reviewers for their constructive comments.

524 **Appendix - Evaluation of the GMI-MERRA simulation**

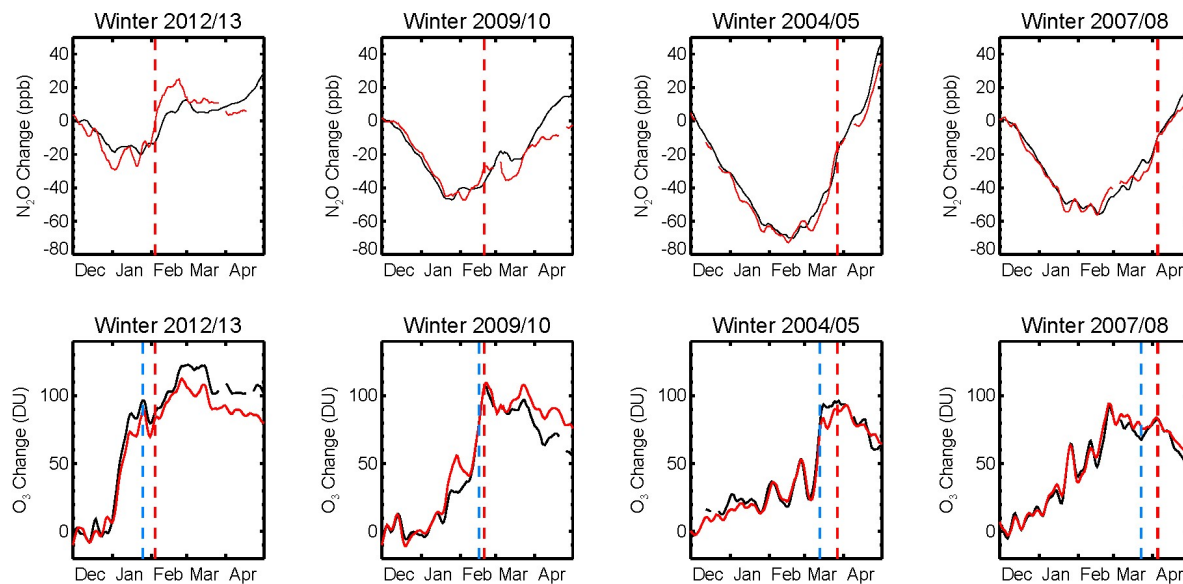
525 Arctic ozone changes during winter are a result of a dynamical (transport) contribution and
526 heterogeneous chemical loss. Both must be realistically represented in order to accurately simulate
527 ozone. We demonstrate the fidelity of the GMI simulation with full chemistry by comparing it with Aura
528 MLS O₃ and N₂O observations. The N₂O comparison is used to evaluate lower stratospheric transport
529 independent of polar ozone chemistry. N₂O changes during winter, averaged over the Arctic cap (63-
530 90°N equivalent latitude), are driven by diabatic descent and meridional mixing. If winter transport is
531 realistic, then the Arctic ozone comparison gauges how well chemical loss is well represented.

532 Figure A1 compares the evolution of Arctic cap average N₂O (450 K) and stratospheric column O₃ for
533 MLS and GMI during winter and spring in 4 years. Each species is plotted as the change with respect to
534 its Arctic cap value averaged over 1-10 December. The years were chosen to show the CTM
535 performance under a wide range of dynamical conditions during the Aura period; they are ordered left
536 to right by the day of the final warming. 2013 had an early January major SSW, 2010 had a mid-February
537 minor SSW, 2005 had a large cold vortex with a March final warming, and 2008 had a small cold vortex
538 with an April final warming. The onset of vortex breakdown is shown by the dashed red line. This was
539 determined by the date when the equivalent latitude of the 450 K vortex edge reached or exceeded 75°,
540 resulting in an area of less than 1/3 of the 63-90° polar cap (< 9 million km²). The dashed blue line is 3
541 days after the final date of temperatures below the chlorine activation threshold, chosen to represent
542 the point when nearly all ozone depletion has ceased. The top row of Figure A1 shows that the seasonal
543 change in GMI N₂O (black) tracks closely with observed changes (red) throughout the winter, indicating
544 a good representation of vortex isolation and descent. Poorer agreement is found after a SSW and after
545 the final warming when mixing with midlatitude air occurs. However, the period of ozone depletion
546 (dates to the left of blue dashed line) show excellent transport fidelity, suggesting that dynamical
547 changes to O₃ that occur during depletion are well-represented. Good agreement between vortex GMI
548 and MLS O₃, N₂O, and ClO is also found in the very cold winter of 2011. This was shown in Strahan et al.
549 [2013] and is not repeated here.

550 The bottom row of Figure A1 shows excellent agreement in all 4 years between MLS and GMI Arctic cap
551 stratospheric column O₃ during the period of ozone depletion. Because transport is well-represented
552 during this period, the excellent agreement between MLS and GMI column O₃ indicates that the
553 chemical loss is also well represented. For the 2005-2015 period, the average difference between MLS
554 and GMI O₃ change during the depletion period is 1 DU with a standard deviation of 8 DU. GMI

555 stratospheric column O_3 also has very good agreement with MLS through the end of March. The average
556 December to March Arctic O_3 change is 77 DU for both MLS and GMI, and one standard deviation of the
557 GMI O_3 error is 8 DU, about 10%. The ability of the simulated column O_3 and lower stratospheric N_2O to
558 closely track the MLS observed changes during winter demonstrates that this simulation is well-suited
559 for the calculation of heterogeneous chemical loss and dynamical contributions to Arctic ozone.

560



561

562 Figure A1. Evaluation of GMI performance in the Arctic during 4 dynamically different winters. All
563 panels compare the seasonal evolution of the Arctic cap (63-90°N EqL) average of GMI (black) and MLS
564 (red) trace gases relative to their value averaged from December 1-10. Top panels show N_2O change (in
565 ppb) on the 450 K surface. Bottom panels show stratospheric column O_3 change (DU). The red dashed
566 line indicates the date of the final warming, which ranges from early February to early April in the 4
567 years. The blue dashed line falls 3 days after the final date of temperatures below the chlorine activation
568 threshold in the lower stratosphere.

569 **References**

- 570 Abalos, M., B. Legras, F. Ploeger, and W.J. Randel (2015), Evaluating the advective Brewer-Dobson
571 circulation in three reanalyses for the period 1979-2012, *J. Geophys. Res.*, 120,
572 doi:10.1002/2015JD023182.
- 573 Andrews, D.G., J.R. Holton, and C.B. Leovy (1987), *Middle atmosphere dynamics*, Academic Press, Inc.,
574 London.
- 575 Bednarz, E.M., A.C. Maycock, N.L. Abraham, P. Braesicke, O. Dessens, and J.A. Pyle (2016), Future Arctic
576 ozone recovery: the importance of chemistry and dynamics, *Atmos. Chem. Phys. Disc.*,
577 doi:10.5194/acp-2015-998.
- 578 Charlton, A.J. and L.M. Polvani (2007), A new look at stratospheric sudden warmings: Part I: Climatology
579 and modeling benchmarks, *J. Climate*, 20, 449-469.
- 580 Chipperfield, M.P. and R.L. Jones (1999), Relative influences of atmospheric chemistry and transport on
581 Arctic ozone trends, *Nature*, 400, 551-554.
- 582 Dameris, M. and S. Godin-Beekmann (2014), Update on global ozone: Past, present, and future, Chapter
583 3 in *Scientific Assessment of Ozone Depletion: 2014*, Global Ozone Research and Monitoring Project
584 – Report No. 55, World Meteorological Organization, Geneva, Switzerland.
- 585 Hanson, D. and K. Mauersberger (1988), Laboratory studies of the nitric acid trihydrate: Implications for
586 the south polar stratosphere, *Geophys. Res. Lett.*, 15, 855-858.
- 587 Kawa, S. R., et al. (1997), Activation of chlorine in sulfate aerosol as inferred from aircraft observations,
588 *J. Geophys. Res.*, 102, 3921-3933.
- 589 Kuttippurath, J. and G. Nikulin (2012), A comparative study of the major sudden stratospheric warmings
590 in the Arctic winters 2003/2004-2009/2010, *Atmos. Chem. Phys.*, 12, 8115-8129.
- 591 Lawrence, Z.D., G.L. Manney, K. Minschwaner, M.L. Santee, and A. Lambert (2015), Comparisons of polar
592 processing diagnostics from 34 years of the ERA-Interim and MERRA reanalyses, *Atmos. Chem.*
593 *Phys.*, 15, 3873-3892.
- 594 Li, F., D.W. Waugh, A.R. Douglass, P.A. Newman, S. Pawson, R.S. Stolarski, S.E. Strahan, and J.E. Nielsen
595 (2012), Seasonal variations of stratospheric age spectra in the Goddard Earth Observing System
596 Chemistry Climate Model (GEOSCCM), *J. Geophys. Res.*, 117, D05134, doi:10.1029/2011JD016877.
- 597 Livesey, N., et al. (2011), Earth Observing System (EOS) Aura Microwave Limb Sounder (MLS) Version 3.3
598 Level 2 data quality and description document, JPL D-33509.

599 Livesey, N.J., M.L. Santee, and G.L. Manney (2015a), A Match-based approach to the estimation of polar
600 stratospheric ozone loss using Aura Microwave Limb Sounder observations, *Atmos. Chem. Phys.*,
601 15, 9945–9963.

602 Livesey, N.J., et al. (2015b), Earth Observing System (EOS) Aura Microwave Limb Sounder (MLS) Version
603 4.2x Level 2 data quality and description document, JPL D-33509 Rev. A.

604 Manney, G.L., L. Froidevaux, M.L. Santee, N.J. Livesey, J.L. Sabutis, and J.W. Waters (2003), Variability of
605 ozone loss during Arctic winter (1991–2000) estimated from UARS Microwave Limb Sounder
606 measurements, *J. Geophys. Res.*, 108, 4149, doi:10.1029/2002JD002634.

607 Manney, G.L., Z.D. Lawrence, M.L. Santee, N.J. Livesey, A. Lambert, and M.C. Pitts (2015), Polar
608 processing in a split vortex: Arctic ozone loss in early winter 2012/2013, *Atmos. Chem. Phys.*, 15,
609 5381-5403.

610 Mueller, R., U. Schmidt, A. Engel, D.S. McKenna, and M.H. Proffitt (2001), The O₃-N₂O relation from
611 balloon-borne observations as a measure of Arctic ozone loss in 1991/92, *Q.J.R. Meteorol. Soc.*,
612 127, 1389-1412.

613 Mueller, R., S. Tilmes, P. Konopka, J.-U. Groos, and H.-J. Jost (2005), Impact of mixing and chemical
614 change on ozone-tracer relations in the polar vortex, *Atmos. Chem. Phys.*, 5, 3139-3151.

615 Mueller, R., J.-U. Groos, C. Lemmen, D. Heinze, M. Dameris, and G. Bodeker (2008), Simple measures of
616 ozone depletion in the polar stratosphere, *Atmos. Chem. Phys.*, 8, 251-264.

617 Nash, E.R., P.A. Newman, J.E. Rosenfield, and M.R. Schoeberl (1996), An objective determination of the
618 polar vortex using Ertel's potential vorticity, *J. Geophys. Res.*, 101, 9471-9478.

619 Newman, P.A., E. R. Nash, and J. E. Rosenfield (2001), What controls the temperature of the Arctic
620 stratosphere during the spring?, *J. Geophys. Res.*, 106, D17, doi:10.1029/2000JD000061.

621 Newman, P.A., S.R. Kawa, and E.R. Nash (2004), On the size of the Antarctic ozone hole, *Geophys. Res.*
622 *Lett.*, 31, L21104, doi:10.1029/2004GL020596.

623 Newman, P.A., E.R. Nash, S.R. Kawa, S.A. Montzka, and S. Schauffler (2006), When will the Antarctic
624 ozone hole recover?, *Geophys. Res. Lett.*, 33, L12814, doi:10.1029/2005GL025232.

625 Newman, P.A., J.S. Daniel, D.W. Waugh, and E.R. Nash (2007), A new formulation of equivalent effective
626 stratospheric chlorine (EESC), *Atmos. Chem. Phys.*, 7, 4537-4552.

627 Newman, P.A. and R. McKenzie (2011), UV impacts avoided by the Montreal Protocol, *Photochem.*
628 *Photobiol. Sci.*, 2011, 10, 1152–1160.

629 Randel, W.J., F. Wu, and R. Stolarski (2002), Changes in column ozone correlated with the stratospheric
630 EP flux, *J. Met. Soc. Jap.*, 80, 849-862.

631 Rex, M., et al. (2002), Chemical depletion of Arctic ozone in the winter 1999/2000, *J. Geophys. Res.*, 107,
632 8276, doi:10.1029/2001JD000533.

633 Rex, M., R.J. Salawitch, P. von der Gathen, N.R.P. Harris, M.P. Chipperfield, and B. Naujokat (2004), Arctic
634 ozone loss and climate change, *Geophys. Res. Lett.*, 31, doi:10.1029/2003GL018844.

635 Rex, M., et al. (2006), Arctic winter 2005: Implications for stratospheric ozone loss and climate change,
636 *Geophys. Res. Lett.*, 33, L23808, doi:10.1029/2006GL026731.

637 Rienecker, M.M. et al. (2011), MERRA: NASA's Modern Era Retrospective Analysis for Research and
638 Applications, *J. Climate*, 24, 3624-3648.

639 Schoeberl, M.R., A.R. Douglass, Z. Zhu, and S. Pawson (2003), A comparison of the lower stratospheric
640 age spectra derived from a general circulation model and two data assimilation systems, *J.*
641 *Geophys. Res.*, 108, doi:10.1029/2002JD002652.

642 Strahan, S. E., A.R. Douglass, and P.A. Newman (2013), The contributions of chemistry and transport to
643 low Arctic ozone in March 2011 derived from Aura MLS observations, *J. Geophys. Res.*, 118, 1563–
644 1576, doi:10.1002/jgrd.50181.

645 Strahan, S.E., A.R. Douglass, P.A. Newman, and S.D. Steenrod (2014), Inorganic chlorine variability in the
646 Antarctic vortex and implications for ozone recovery, *J. Geophys. Res.*, 119,
647 doi:10.1002/2014JD022295.

648 Tan, W.W., M.A. Geller, S. Pawson, and A. DaSilva (2004), A case study of excessive subtropical transport
649 in the stratosphere of a data assimilation system, *J. Geophys. Res.*, 109, D11102,
650 doi:10.1029/2003JD004057.

651 Tegtmeier, S., M. Rex, I. Wohltmann, and K. Krueger (2008), Relative importance of dynamical and
652 chemical contributions to Arctic wintertime ozone, *Geophys. Res. Lett.*, 35, L17801,
653 doi:10.1029/2008GL034250.

654 Tilmes, S., R. Mueller, J.-U. Grooss, D.S. McKenna, J.M. Russell III, and Y. Sasano (2003), Calculation of
655 chemical ozone loss in the Arctic winter 1996–1997 using ozone-tracer correlations: Comparison of
656 Improved Limb Atmospheric Spectrometer (ILAS) and Halogen Occultation Experiment (HALOE)
657 results, *J. Geophys. Res.*, 108, 4045, doi:10.1029/2002JD002213.

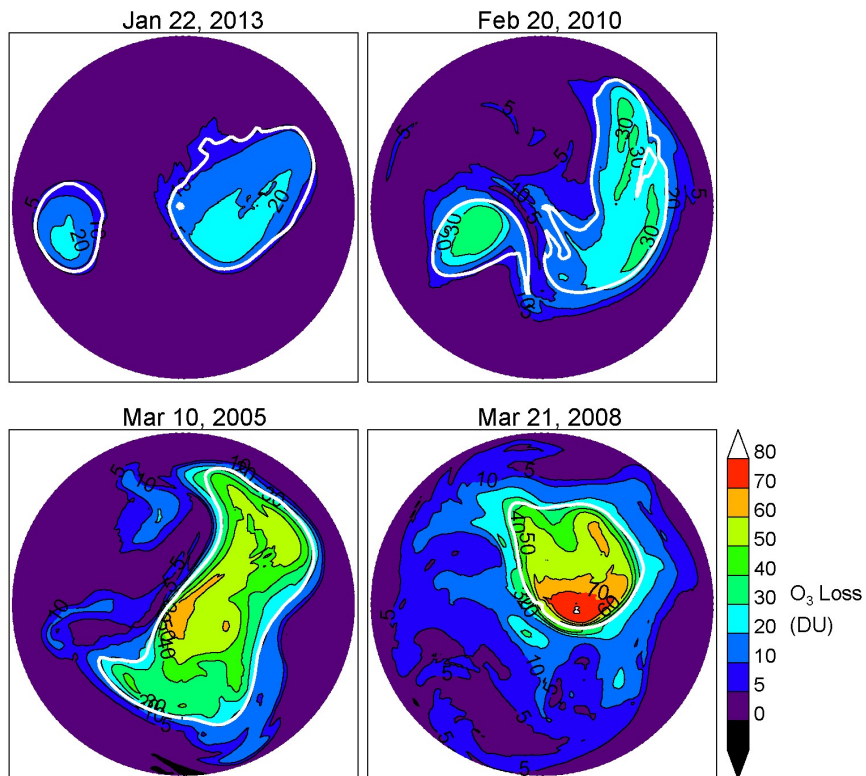
658 Weber, M., S. Dhomse, F. Wittrock, A. Richter, B.-M. Sinnhuber, and J.P. Burrows (2003), Dynamical
659 control of NH and SH winter/spring total ozone from GOME observations in 1995-2002, *Geophys.*
660 *Res. Lett.*, 30, 1583, doi:10.1029/2002GL016799.

661 Weber, M., S. Dikty, J.P. Burrows, H. Garny, M. Dameris, A. Kubin, J. Abalichin, and U. Langematz (2011),
662 The Brewer-Dobson circulation and total ozone from seasonal to decadal time scales, *Atmos. Chem.*
663 *Phys.*, 11, 11221-11235.

664 Wohltmann, I., et al. (2013), Uncertainties in modelling heterogeneous chemistry and Arctic ozone
665 depletion in the winter 2009/2010, *Atmos. Chem. Phys.*, 13, 3909-3929.

666 WMO (World Meteorological Organization) (2014), *Scientific Assessment of Ozone Depletion: 2014*,
667 *Global Ozone Research and Monitoring Project – Report No. 55*, 416 pp., Geneva, Switzerland.

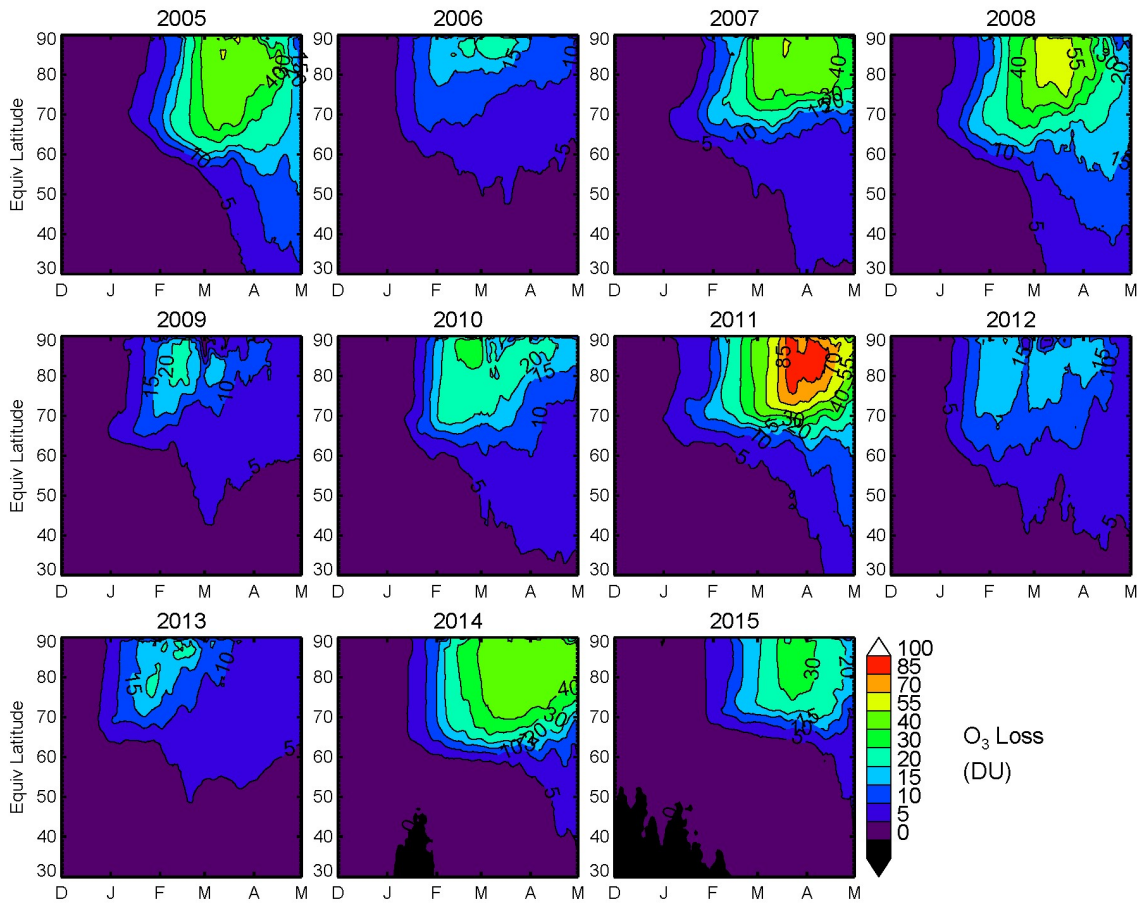
668



670

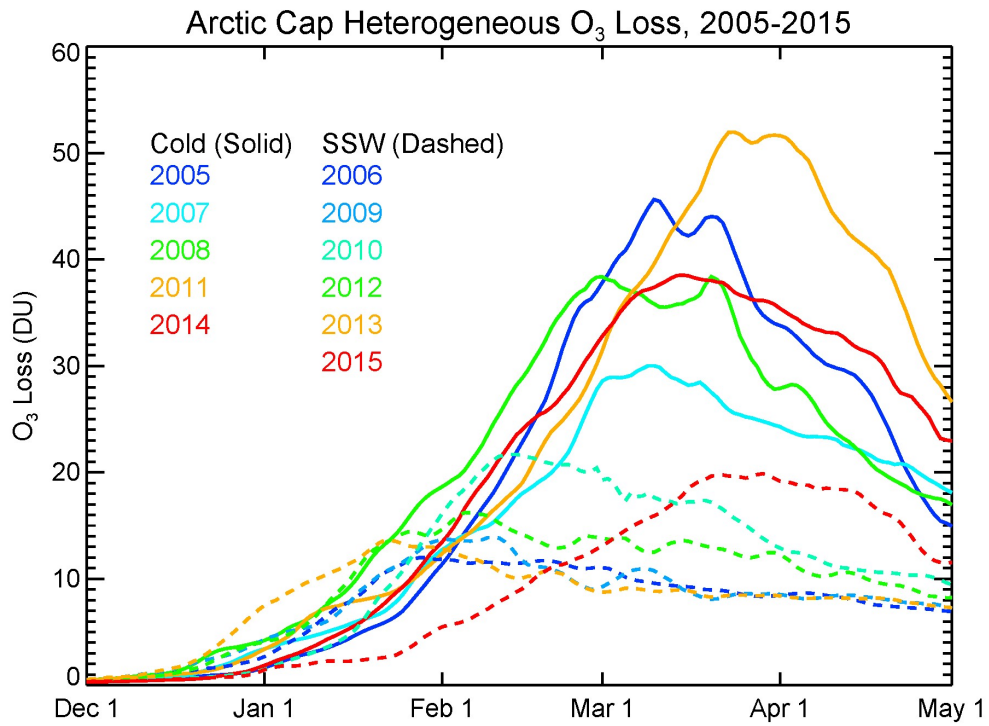
671 Figure 1. Total column heterogeneous chemical ozone loss in Dobson units calculated from GMI
 672 simulations in 4 dynamically different years. The top panels show dynamically disturbed years while the
 673 bottom panels show dynamically quiet years with a longer-lived vortex. Each date chosen shows Arctic
 674 ozone depletion near its seasonal maximum for that year. The white contour indicates the edge of the
 675 450 K polar vortex as defined by the region of maximum potential vorticity gradients [Nash et al., 1996].

676



677

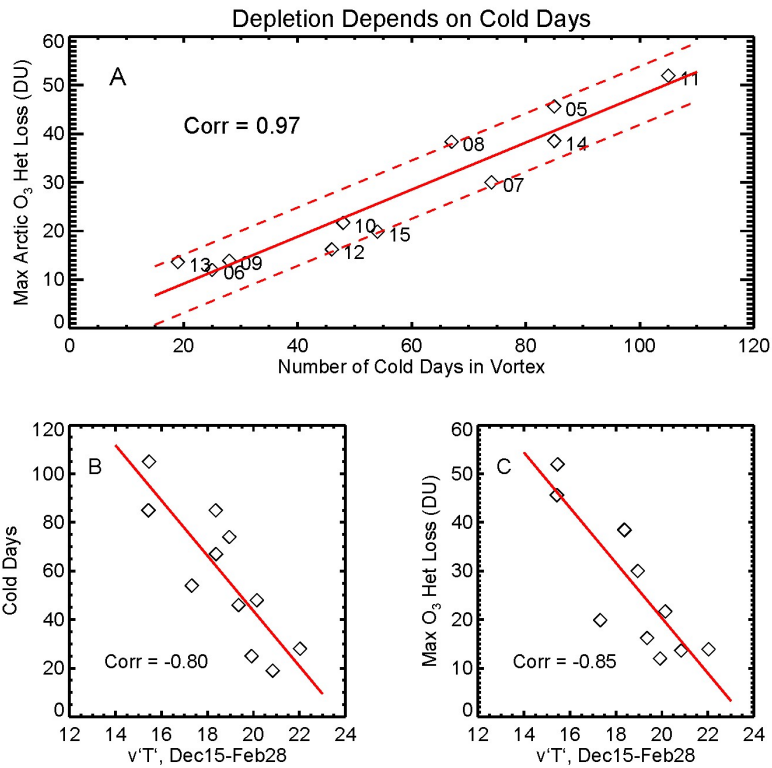
678 Figure 2. Daily total column heterogeneous chemical ozone loss (DU) from the GMI simulations,
 679 December to May for all years 2005-2015 as a function of equivalent latitude. The years with losses >40
 680 DU have a much larger impact on the midlatitudes in spring.



681

682 Figure 3. Time series of Arctic cap average (63-90°N EQL) heterogeneous chemical O₃ losses for 11 years.

683 The results shown used 5-day smoothing.



684

685 Figure 4. a) The linear relationship between the maximum Arctic cap column ozone depletion and the
 686 number of cold days in the Arctic lower stratospheric vortex. The correlation of the 11 points is 0.97. The
 687 dashed lines are ± 6 DU of the fitted line. The number of cold days b) and the maximum ozone
 688 heterogeneous loss c) are both significantly correlated with wave driving (the 45-75°N zonal mean 100
 689 hPa heat flux, $v'T'$, in units of Kms^{-1}) averaged over Dec 15-Feb 28.

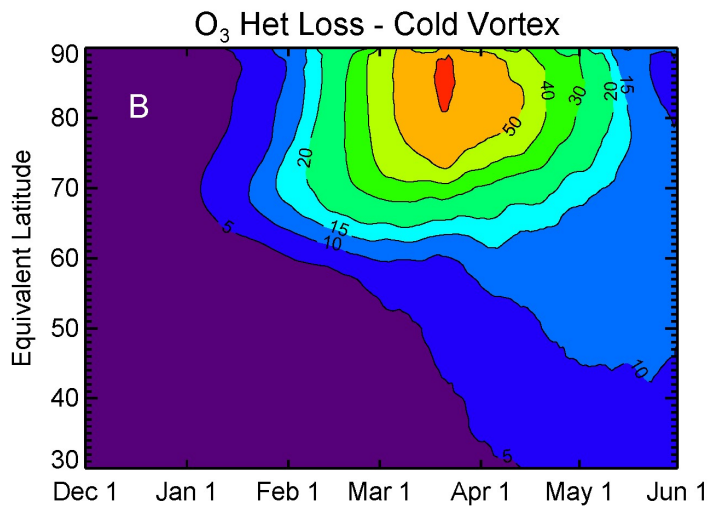
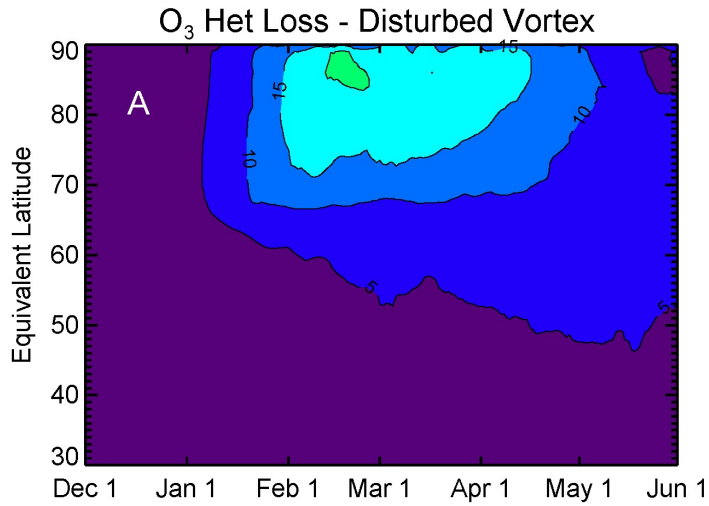
690

691

692

693

694



695

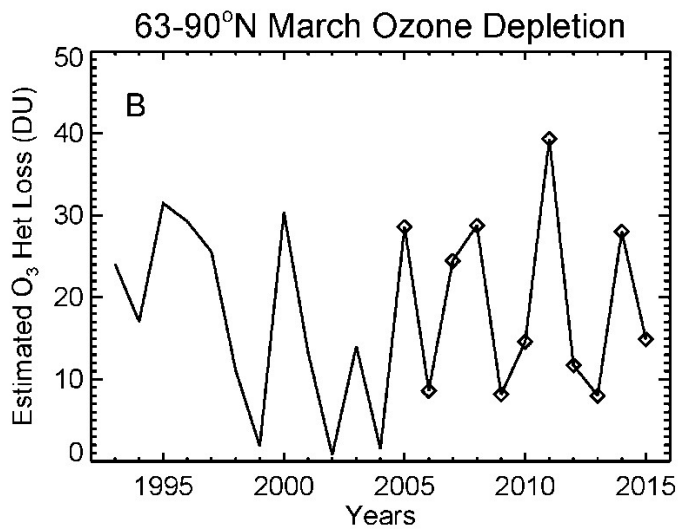
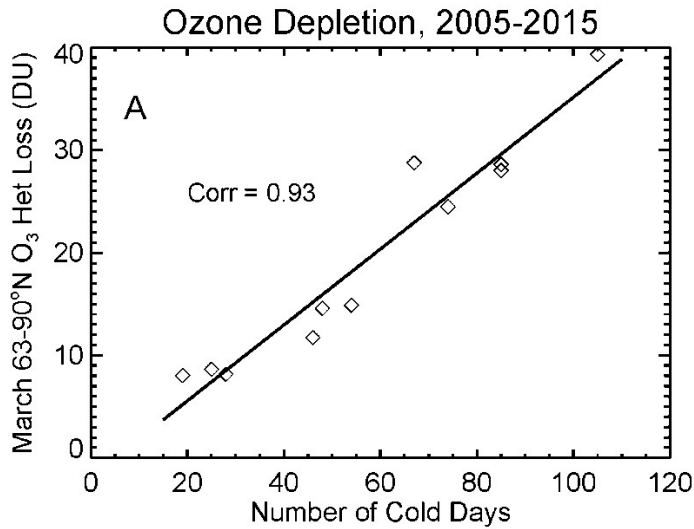
696 Figure 5. The average column ozone depletion (DU) for a) 6 years with SSWs and b) 5 years with no
 697 major or minor SSW before mid-February. The maximum depletion in years without a midwinter
 698 warming is roughly 3 times greater than years with a warming.

699

700

701

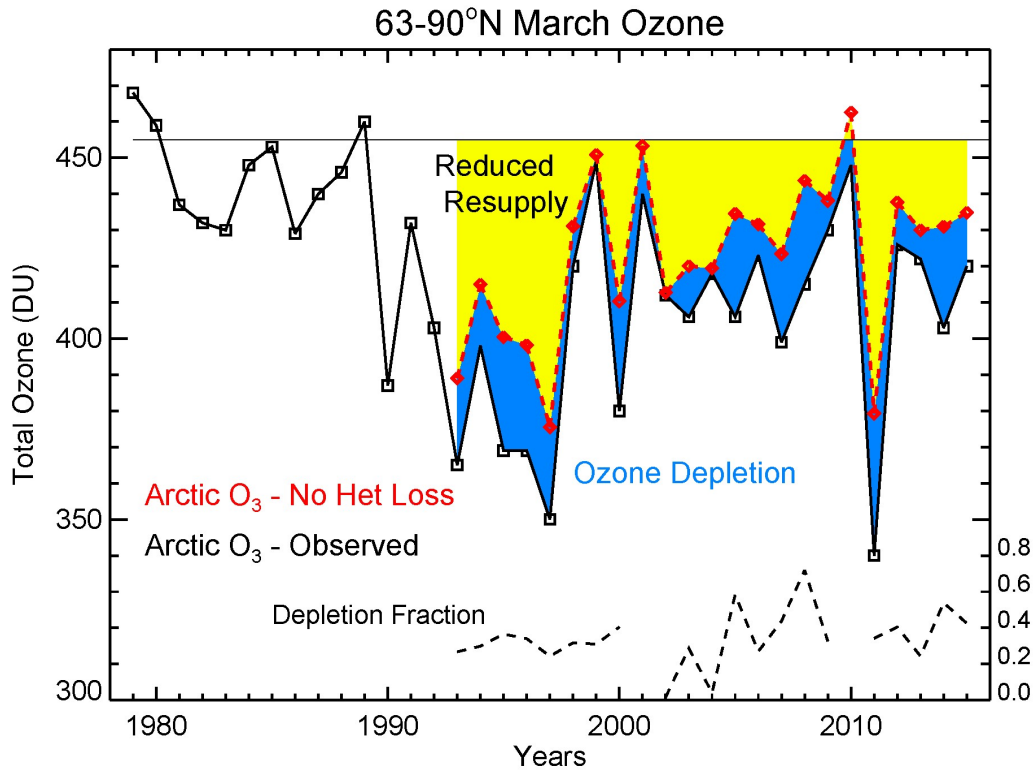
702



703

704 Figure 6. a) The relationship between the number of cold days each winter and the March average
 705 ozone depletion (DU) average over the geographic pole, 63-90°N. This is the basis for estimating O₃
 706 depletion for years prior to the Aura period. b) The estimated geographic polar cap March average
 707 depletion (DU) for years 1993-2004 calculated with the slope of the fitted line in a) and the number of
 708 cold days determined from the MERRA reanalysis. Polar cap loss for 2005-2015 (diamonds) was
 709 calculated with the GMI simulations (i.e., the points in panel a)).

710



711

712 Figure 7. The 63-90°N March average total column O₃ from satellite observations, 1979-2015 (black).
 713 The red dashed line shows the 'No Het Loss' O₃, calculated as the sum of the observed column O₃ and
 714 the loss estimates in Fig. 6b. The amount of loss each year is shown by blue shading. The thin line at 455
 715 DU comes from the WMO [2014] figure and represents their assumed climatological mean value for
 716 March O₃. The difference between the 'No Het Loss' O₃ and 455 DU (yellow shading) shows the impact
 717 of wave driving on resupply. The amount of depletion (blue) with respect to the observations' difference
 718 from 455 DU (yellow+blue) is shown as a dashed line near the bottom.

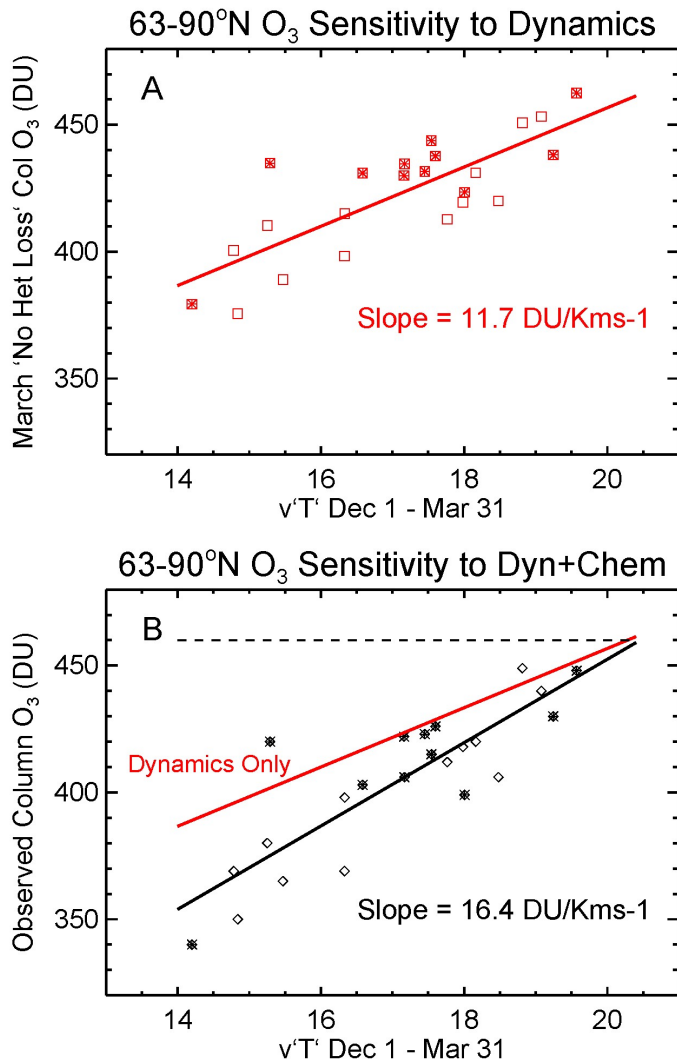
719

720

721

722

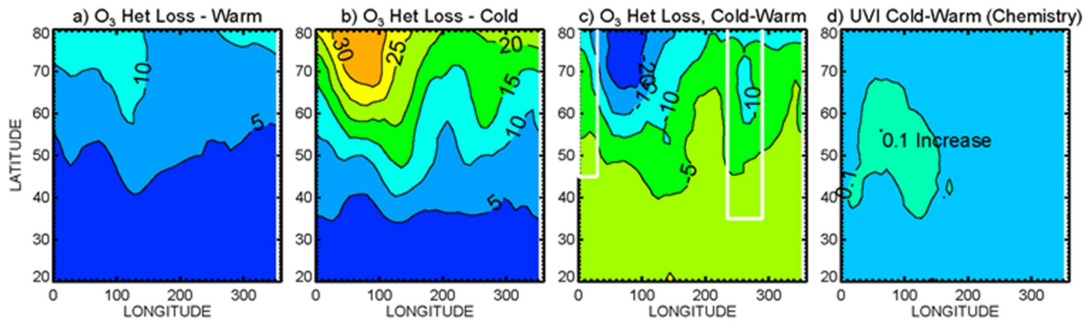
723



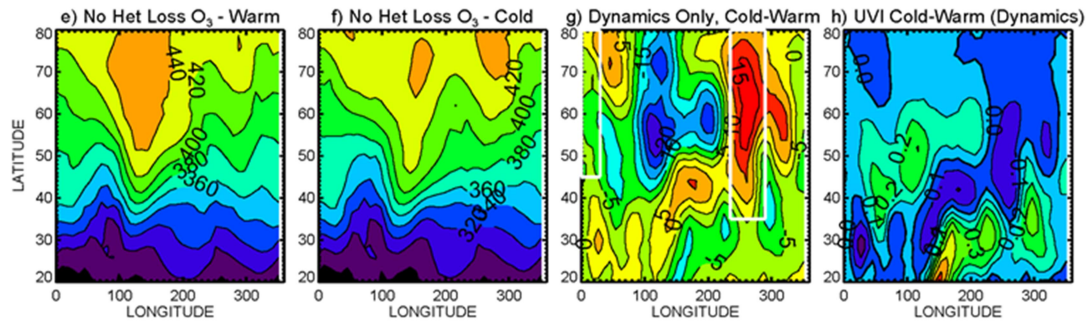
724

725 Figure 8. a) The relationship between March mean 'No Het Loss' column O₃ (DU), 63-90°N, and the
 726 mean heat flux (Kms⁻¹) averaged Dec 1-Mar 31, the period when wave driving influences March O₃. The
 727 slope of the best fit line (red) quantifies the sensitivity of polar O₃ resupply to wave driving. b) The
 728 relationship between observed March mean column O₃ and the mean heat fluxes (black). The slope of
 729 this line shows the combined sensitivities of O₃ resupply and chemical loss to wave driving. The
 730 dynamics-only line from panel a) is shown in red. The intersection of these lines near 460 DU represents
 731 the point where wave driving is sufficient to inhibit heterogeneous loss. For both panels, open symbols
 732 are 1993-2004, filled symbols are 2005-2015.

SSW Impacts on Depletion



SSW Impacts on Resupply



733

734 Figure 9. Separation of the effects of depletion and dynamics on April mean column O₃ after cold and
 735 warm winters 20-80°N latitude, 0-360°E longitude. Panels a)-c) show mean depletions after warm and
 736 cold Arctic winters, and their difference, calculated from the GMI simulations with and without
 737 depletion. Panels e)-g) show warm and cold winters' dynamical effects, and their differences, using the
 738 MLS 'No Het Loss' total column O₃ (see text) in order to identify the impact on O₃ distributions. Panels d)
 739 and h) show the difference in impacts of depletion (d) and dynamics (h) on UV index after cold and
 740 warm winters. The April mean clear sky UVI ranges from 10 at 30°N, 3 at 60°N, and 1-3 in the Arctic.